Evidence of Faradaic Reactions in Electrostatic Atomizers

A. Sankaran[1], C. Staszel[1], R.P. Sahu[1,2], A.L. Yarin[*1], F. Mashayek[1]

[1]Department of Mechanical and Industrial Engineering, University of Illinois at Chicago,

842 W. Taylor St., Chicago IL 60607-7022, U.S.A.

[2]Department of Mechanical Engineering, McMaster University, 1280 Main Street West,

Hamilton, Ontario L8S 4L7, Canada.

Abstract

Any rational theory of the electrostatic atomizers (EA) would require detailed understanding of the nature of the polarized near electrode layer, since this is the source of the electric charge carried by the jets issued from the EAs. The polarized layer either is driven out as the electrically-driven Smoluchowski flow and/or entrained by the viscous shear imposed by the bulk flow. The standard Gouy-Chapman theory of polarized diffuse layers implies zero electric current passing across the layer, which is impossible to reconcile with the fact that there are leak currents in the EAs. Here, we show that the electric current through the EA is controlled by faradaic reactions at the electrodes. The experiments were conducted with stainless steel or brass pin-like cathodes and three different anode (the conical nozzle) materials, which were copper, stainless steel and brass. The different electrode materials resulted in different spray, leak and total currents in all the cases. Accordingly, it is shown that the total electric current generated by EAs

* Correspondence should be addressed to E-mail: ayarin@uic.edu. Phone: +1(312) 996-3472. Fax: +1(312) 413-0447.

.

can be controlled by the cathode and anode materials, i.e. by faradaic reactions on them. This lays the foundations for a more detailed understanding and description of the operation of EAs.

Introduction

Electrostatic atomization is an emerging technology with numerous applications, namely: spray combustion, painting, spray coating, pesticide control, etc.[1-7] This technology employs the electric charging of the liquid flowing through an EA, and thus the electric charging of a jet/spray issued from its nozzle. One of the unique benefits of charged drops in sprays is the secondary atomization when an evaporating drop reaches the Rayleigh limit[8-10]. The Maxwell stress acting on a charged drop pulls its surface outwards due to the attraction of the free charges at the surface to a grounded electrode at infinity. Thus, the Maxwell stress effectively diminishes the capillary pressure, $2\sigma/a$, with σ being the surface tension and a being the effective drop radius, which essentially means that in the presence of the Maxwell stress the effective surface tension is reduced, and drop fission in the course of its oscillations is facilitated. Note, that secondary atomization of a drop in flight after surpassing the Rayleigh limit was observed in Ref. 11. As a result, tiny droplets are formed from the primary drops via the electrically-driven instabilities. Also, the electric repulsion greatly enhances drops dispersion in sprays[5], facilitates directional control of drops by means of the applied electrical fields[5], diminishes the over-sprays prevalent in many painting applications[6], and facilitates spray formation without application of high pressure or the use of heated oils[6]. An interesting recent biomedical application involving formation of nano- and pico-sized droplets

utilizing pyro-electro-hydrodynamic method[12, 13] ascertains the relevance of electro-hydrodynamic processes in forming extremely tiny droplets.

The initial work on EAs involved sharp metal electrodes located inside insulating capillary tubes[8, 14], while the grounded electrode was a collector surface typically located far from the charged metal electrode. As a result, the electrified flows generated by such devices proved to be inappropriate for the industrial applications due to the low flow rates required for sufficient charging. These designs were subsequently augmented by adding an additional grounded metal counter-electrode near the sharp electrode[5-7,15]. This successful modification significantly increased the resultant electrification and charge appearance in the issued jet/spray, which delivers the so-called electric spray current. It should be emphasized that with the introduction of the grounded electrode close to the charged electrode, the leakage current exists between them, i.e. the overall current splits into the leakage and spray currents. The leakage current is essentially an electrical loss from the electrostatic atomization point of view.

Various experimental works have been conducted on such EAs to study the governing parameters, aiming to increase the spray current, while decreasing the leakage current[5-7, 16]. For example, several works[5-7, 16] studied the effect of parameters such as the orifice diameter, flow rate, and the electrical parameters, trying to elucidate simple scaling rules to optimize and predict the resultant spray current and the corresponding specific electric spray charge. Some other studies were concerned with the charged jet breakup and the resulting droplet characteristics[17-19].

The mechanism of liquid electrification is still debated. One method of charge injection, the direct or unipolar charge injection, has been studied utilizing a corona

discharge to impart ions into leaky dielectric liquids[20]. Traditionally, non-polar liquids are considered insulators. However, these liquids possess ions typically of unspecified origin, possibly due to the presence of dissociated admixtures, resulting in a relatively low conductivity[21, 22]. For this reason, these liquids are called leaky dielectrics[4, 23, 24].

A number of studies implied the occurrence of faradaic reactions at the electrode interfaces[6, 15, 25]. It is known that, in general, the electric currents in electrolytes can be either diffusion-limited or kinetics-limited[26]. The diffusion-limited regime corresponds to the case of very fast faradaic reaction compared to the diffusion and electro-migration of ions to the electrode, which results in the "dry-out" of the latter, i.e. the ion concentration reaching zero, which in turn would prevent any further electric current[26]. On the other hand, in the kinetics-limited regime, the rate of faradaic reaction is much slower than the diffusion and electro-migration of ions to the electrode[26]. The kinetic analysis of charge origination and conduction in non-polar liquids is also reported[27]. It was observed that charge transport in corn oil might be controlled by faradaic reactions in the kinetics-limited regime[28], which implies a sluggish nature of heterogeneous reactions at the electrodes in the case of leaky dielectrics[29]. The potential effect of the electrode material on the charge transfer in EAs was never studied experimentally[24].

The aim of the present work is to investigate the effect of the electrode material on both spray and leakage currents in EA. In previous works[5-7], the only electrode materials used were stainless steel or tungsten for the pin electrode, and brass or stainless for the counter-electrode nozzle. There was no discussion at all on whether the electrohydrodynamics of EAs are affected by the electrode material choice and how that is related to the underlying physical mechanisms. These issues are addressed in the

present study. The first part of the article describes the experimental setup. Next, characterization of the electrode surfaces is discussed. After that, the results are presented and discussed, including the link to faradaic reactions in the framework of the Volmer-Butler model. Finally, the conclusions are drawn.

Experimental

The schematic of the electrostatic atomizer used in this study includes an air pressure regulator, pressure chamber, atomizer, metal collector, high voltage supply, weighing balance, 1 MΩ external resistor, and multimeter as illustrated in Figure 1. The EA used a sharp pin electrode made either from brass (alloy 360) or stainless steel (alloy 303). The electrode was inserted into the nozzle chamber (cf. Figure 1), made of brass and guided through the central hole of an insulating disc made of Polyether ether ketone (PEEK) placed concentrically to the nozzle chamber. Also, the guide plate had five circular openings, 6.35 mm in diameter, which ensured its high permeability of the oil flow toward the nozzle.
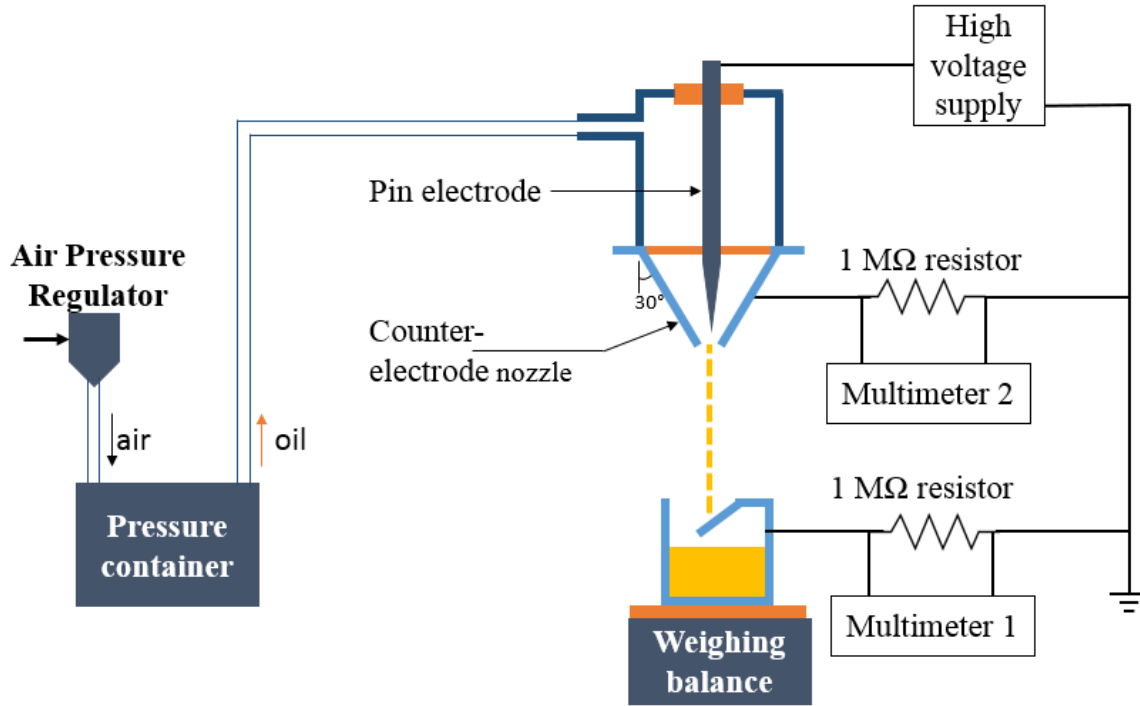
Figure 1. Schematic of the experimental setup of the electrostatic atomizer used to measure the I-V characteristics at varying high voltages.

The counter-electrode, i.e. the nozzle, with the 30° angle at the virtual tip was bolted to the cylindrical part of the nozzle chamber. The materials used for the counter electrode were brass (alloy 360), stainless steel (alloy 303), or copper (alloy 110). The pin electrode was insulated from the nozzle chamber using PEEK of 6 mm annular thickness. The axial distance between the pin electrode and the tip of the converging counter-electrode nozzle was set to 3.175 mm (which corresponds to the 1.8 mm nearest distance between the electrodes) by a spring-loaded micrometer with a resolution of 0.001 mm. The electrostatic atomizer was mounted on a Delrin insulating holder. The pin electrode was connected to a custom-built negative high voltage (0-20 kV) DC supply.

The pressure regulator maintains a constant pressure, thus maintaining a steady-state oil supply into the atomizer. The oil exiting the atomizer as a jet was collected into an insulated collection vessel placed on a weighing balance using a sheet of Teflon. The oil jet impinged onto an inclined metal plate to avoid splashing. The metal plate was connected to a 1 MΩ external resistor in parallel to the multimeter 1 (Fluke model 8845A). The spray current I_S through the resistor was obtained using Ohm's law. The leakage current I_L from the nozzle was measured through the voltage drop across 1 MΩ resistor connected in parallel to the multimeter 2 (HP model 3478A). The total current is the sum of the spray and leakage currents. The leakage and spray currents, were recorded at a frequency of 1Hz using Labview and Flukeview respectively. The multimeters had a resolution of 100 nV. The volumetric flow rate was measured by the weighing balance using the mass of oil collected during a certain time interval and the oil density.

Six different atomizer configurations (the stainless steel and brass pin electrode with three different metals of the counter-electrode nozzle) were studied in two separate sets of experiments to elucidate the effect of the electrode materials on the spray, leakage and total currents. In the first set the current-voltage (I-V) characteristics were studied at different high voltages varying from -4.0 kV to -12.0 kV. These tests are termed the I-V characteristics. The electrostatic atomizer (EA) in each of the six different configurations was operated at voltages applied to the pin electrode starting at -12 kV, then increased in the increments of 1.0 kV. The EA was operated for 300 s at each voltage setting, and the corresponding spray and leakage currents were recorded every second. In the case of the EA with the brass pin electrodes and the counter-electrode nozzles of brass, stainless steel, or copper, the experiments were conducted up to -4.0 kV, -5.0 kV, -7.0 kV,

respectively. In the case of the stainless steel pin electrode with the counter-electrode nozzles of brass, stainless steel, or copper, the experiments were conducted up to -4.0 kV, -5.0 kV, -8.0 kV, respectively. The choice of these voltages stemmed from the spray current reaching such low values that multimeters 1 in Figure 1 would reach their accuracy limit. A maximum voltage of -12 kV was chosen since corona discharge in the setup was observed to occur at around -12.5 kV. To prevent damaging the setup, the voltages surpassing -12.0 kV were not used.

In another set of experiments, termed the fixed voltage experiments, the high voltage was set at -12.0 kV and multiple trials were conducted for different configurations of the electrode and the nozzle materials as mentioned above. The choice in these voltages stemmed from the spray current reaching low values where the multimeter would reach its limit of accuracy. A maximum of -12 kV was chosen, since corona discharge in the system was observed to occur at around -12.5 kV. To prevent damaging the system, voltages above -12.0 kV were not employed.

In the experiments with the first setup shown in Figure 1 the largest standard deviation in the current values was observed at the largest-by-magnitude voltage of -12.0 kV. Since the experiments with the fixed voltage were planned at this voltage, the setup was modified by including an upgraded flow control unit as shown in Figure 2. In this case, the flow rate was regulated by a rotameter (Cole Parmer, model EW-03267-90) with a 150 mm scale and 1 mm as the least gradation. The rotameter was calibrated using a graduated cylinder. In addition, a polypropylene filter holder (Advantec model 43303020) containing a glass fiber filter (Advantec model GD-120) was attached in line,

after the pressure container (cf. Figure 2). An ultra-precision needle valve (McMaster-Carr model 7836K25) was used to control the flow rate as precisely as possible.
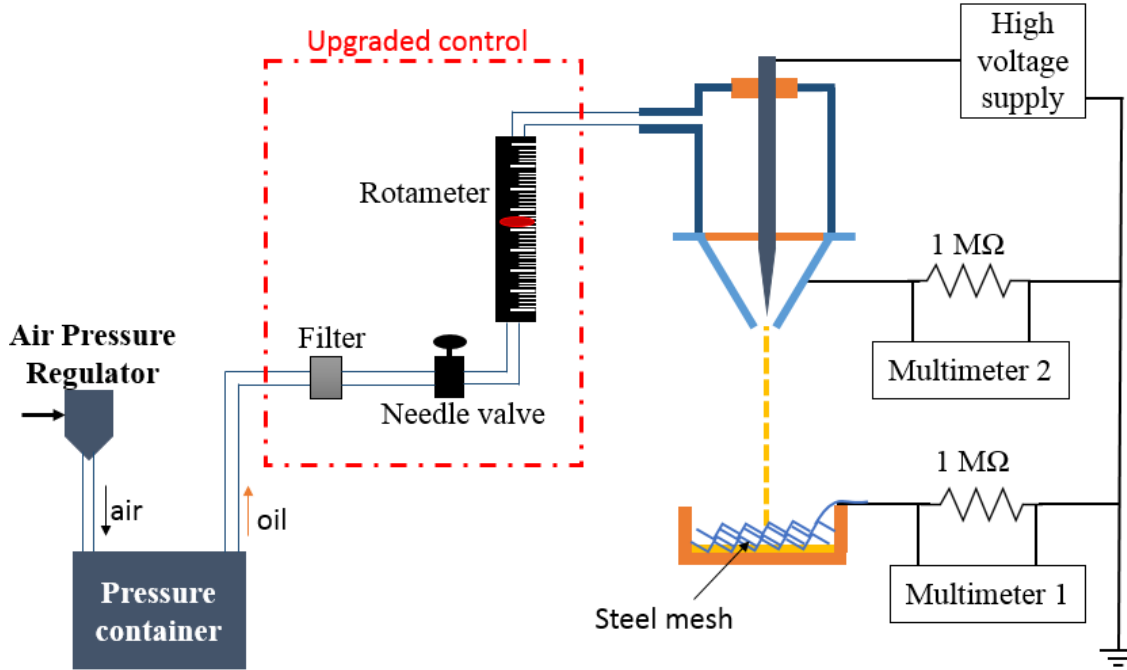

Figure 2. Schematic of the modified experimental setup of the electrostatic atomizer used to measure the current at a constant voltage of -12.0 kV for different materials of the nozzle and the pin electrode.

An additional upgrade to the experimental setup consisted of a thick stainless steel metal mesh collector insulated from the ground in contrast to the setup in Figure 1. The oil jet, after impinging onto this metal mesh, flowed out of the insulated collection vessel located below. The stainless steel metal mesh was connected to a 1 MΩ resistor similar to Figure 1.

As in the I-V characteristics experiment, the spray and leakage currents were measured using the resistors connected to the metal mesh and the counter-electrode

nozzle. In this set of experiments a fixed cathode voltage of -12 kV was applied and 7 trials for each of the six possible EA configurations were conducted to reach reliable statistics. The resultant time averaged spray current, I_S, and the leakage current, I_L, were ensemble averaged.

Electrode characterization

In spite of the precautions described above, corona discharge was observed before conducting experiments of the second type with only the stainless steel pin electrode. This lead to changes in the electrode tip shape. The electrode tip was regularly inspected in two chosen perpendicular directions using the optical microscope (Olympus BX51) at $10\times$ magnification. After corona discharge occurred before the experiments of the second type with the stainless steel pin electrode, a slight change in the electrode tip was observed. This change in the electrode tip is depicted in Figure 3. Here it is observed that the sharp imperfection on the tip had been slightly smoothened, cf. Figures 3b1 and 3b2. However, during the entire experiments of both types no visible changes in the electrode tip were observed for any material of the counter-electrode, i.e. the body of the nozzle. This was confirmed by overlaying the optical images of the electrode tips between experiments in Photoshop, which revealed that the imperfection radii did not change. In the experiments with the brass pin electrode corona discharge never happened, and no changes in the electrode were observed, cf. Figure 4.
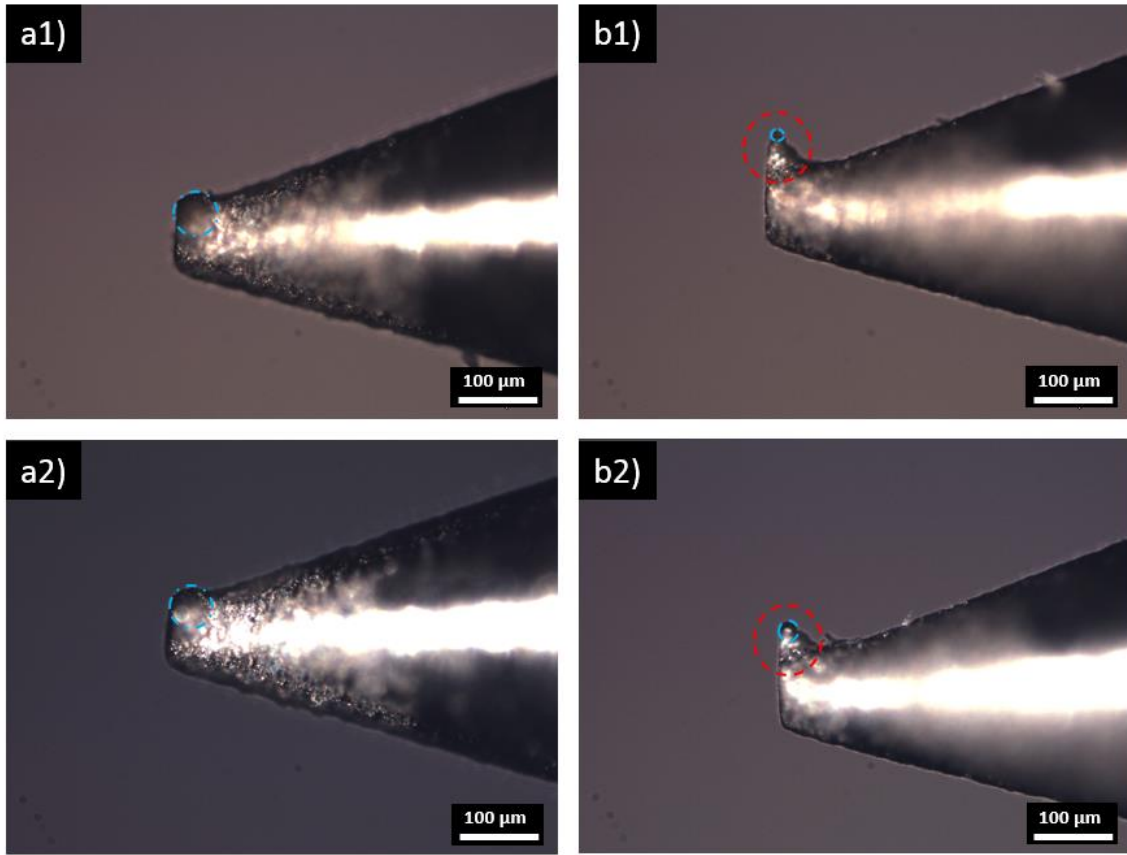
Figure 3. Shape of the tip of the stainless steel pin electrode observed in two perpendicular directions after the experiments of the first type [panels (a1) and (b1)], and of the second type [panels (a2) and (b2)], in which corona discharge could occur. Note the slightly smoothened imperfection of the electrode tip in one direction, highlighted by dashed red circle. The blue circle shows the imperfection radius. The perpendicular directions were chosen by swirling the horizontally located electrode under the microscope.
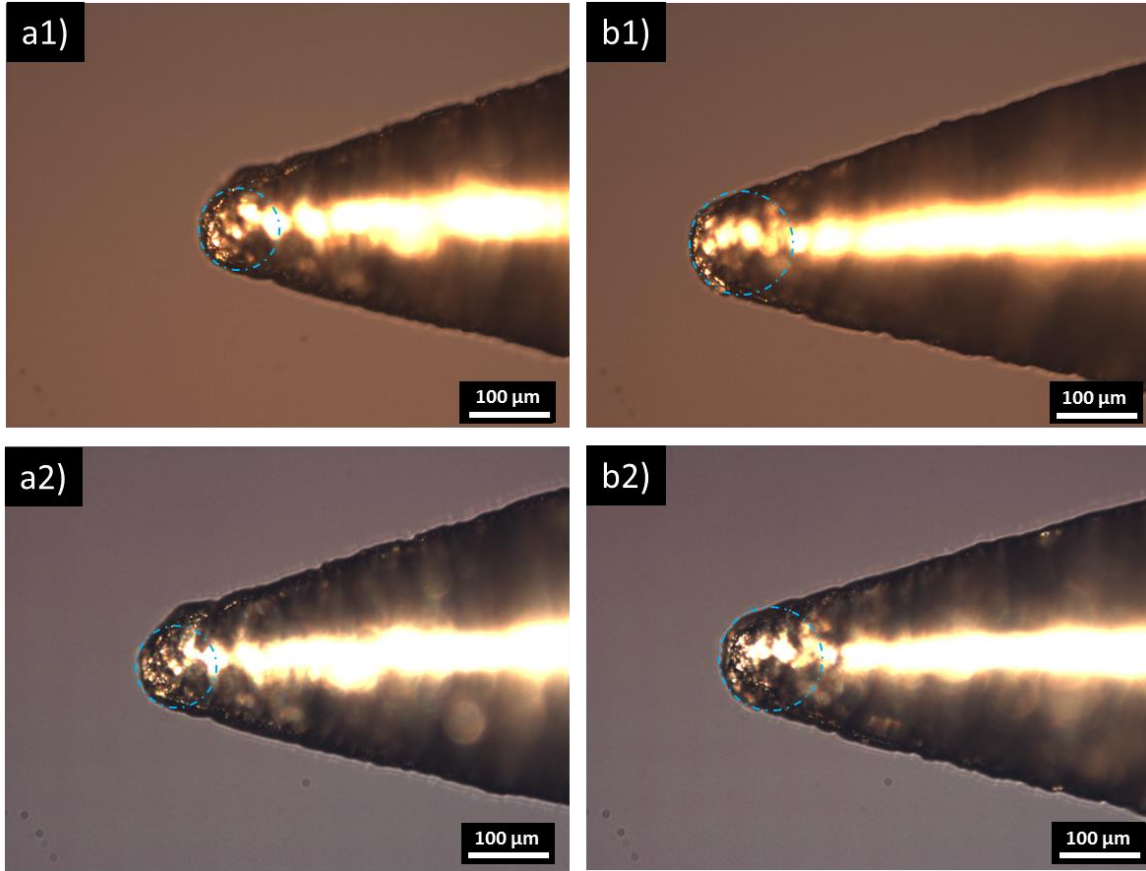
Figure 4. Shape of the tip of the brass pin electrode observed in two perpendicular directions before [panels (a1) and (b1)] and after [panels (a2) and (b2)] the experiments of the first type. The blue circle shows the tip radius. The perpendicular directions were chosen by swirling the horizontally located electrode under the microscope.

Since the electrode tips were rather asymmetric due to the manufacturing imperfections, the imperfection radii were measured as the smallest radii visible in the two perpendicular directions (cf. the images in Figures 3 and 4). The imperfection radii of curvature for the stainless steel pin electrode were $R_{a1}=27$ µm and $R_{b1}=7$ µm, cf. Figures 3a1 and 3b1. After corona discharge, the electrode tip was slightly smoothened, the

corresponding radii were $R_{a2}=27$ µm and $R_{b2}=12$ µm, cf. Figures 3a2 and 3b2. For the brass pin electrode the radii were $R_{a1}= R_{a2}=65$ µm to $R_{b1}= R_{b2}=55$ µm**,** cf. Figures 4a1, 4a2 and 4b1, 4b2.
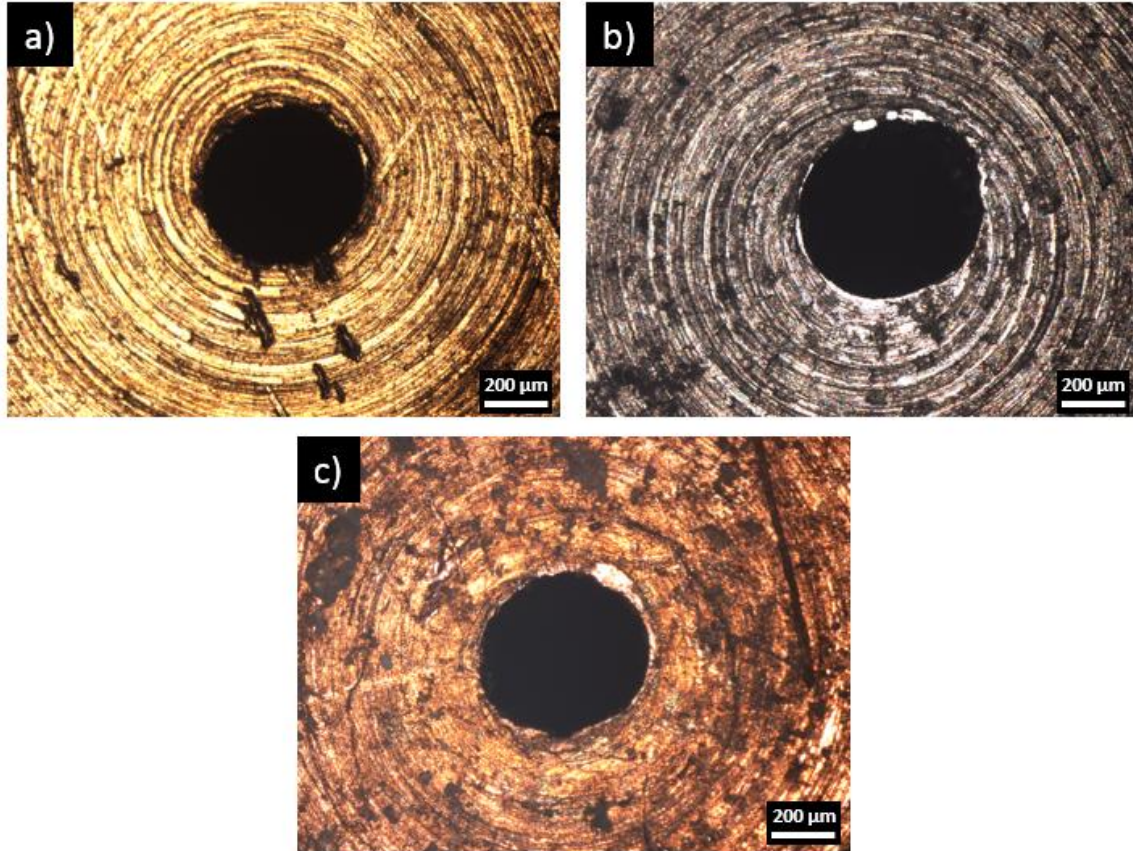

Figure 5. Optical images of the counter-electrode nozzles. Panels (a), (b), and (c) correspond to the brass, stainless steel, and copper counter-electrode nozzles, respectively.

The optical images of the counter-electrode nozzle orifices were obtained at $4\times$ magnification. Figure 5 reveals that for the three metals of the nozzle orifices, the radii were slightly different. For the brass counter-electrode nozzle, the radius of the exit

orifice was 510 µm, for the stainless steel counter-electrode it was 570 µm, and for the copper one it was 530 µm. Different nozzle metals also revealed different roughnesses visible in Figure 5. These differences, in principle, can affect the electric charge transfer and/or the shear stress imposed on the flowing oil, albeit these effects can probably be neglected in the first approximation.

The composition of the electrode materials is listed in Table 1. The faradaic reactions, the standard electrode potentials and work functions of these metals are available in standard handbooks[29-32.]

Table 1. The composition[30] of the electrode materials.

Electrode material	Percentage composition						
Brass	Copper (Cu)			Zinc (Zn)		Lead (Pb)	
	61.5%			35.5%		3%	
Stainless steel	Fe	Cr	Ni	Mn	Si	Mo	C
	69.25%	18%	9%	2%	1%	0.60%	0.15%
Copper	Cu				O		
	99.9%				0.04%		

Results and Discussion

The effect of different materials of the pin electrode and counter-electrode nozzle on both leakage and spray currents of the EA was revealed by using two different sets of experiments, i.e. the one with varying voltage for the I-V characteristics, and another one with the fixed voltage as discussed below.

The I-V Characteristics. In this set of experiments the I-V characteristics of the EA were studied for both brass and stainless steel pin electrodes and three different materials of the counter- electrode nozzle at varying voltages. A 18.93 liter (5 gallon) canister of a food-grade canola oil was used as a working fluid. This canister is referred to as oil batch 1. The food-grade canola oil from batch 1 was pumped into the EA by air pressure from the pressure container which contained a maximum volume of 3.79 liter (one gallon).

The exit jet flow rate, Q_v, was set at around 0.9 mL/s for all the EA configurations used. The flow rate was measured during each trial, and was averaged over the course of the trial. During the experiments, the flow rate would decrease slightly for each subsequent trial, when the voltage was increased (its magnitude decreased, negative voltage), i.e. as more experiments were conducted, the flow rate would decrease by at most 5.6%. This was due to the pressure regulator's inability to sustain a constant pressure inside the pressure container during an experiment. This decrease in the flow rate was detected for each EA configuration, and thus affected the results for all these configurations identically, i.e., at the same set voltage. The flow rate in all these configurations would be comparable and would decrease by a similar value. Thus, this had a negligible effect, if any, on the discussion of the results, which is only concerned with the comparative values.

Multiple trials for a single EA configuration could not be effectively conducted in this set of experiments due to the limited amount of oil in each batch. The reason for using only a single batch of canola oil was our observation that oil from different canisters would result in significantly different spray, leakage and thus total currents.

This was likely due to the uncontrolled differences in production of different batches of oil, which resulted in their different electric conductivity properties. Accordingly, all the oil used in the experiments of the first type to measure the I-V characteristics was obtained from a single batch of oil, denoted as batch 1.

It should be emphasized that in all cases of the six different EA configurations, only charged jets rather than sprays were issued from the EA (cf. Figure 6). However, the
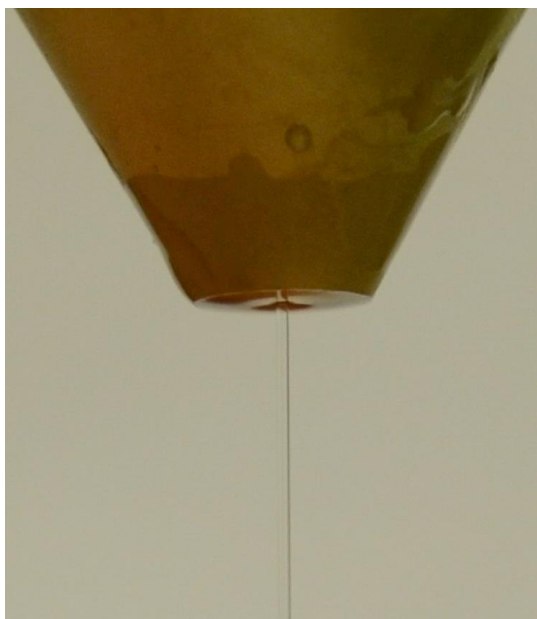

Figure 6. Charged oil jet issued from the counter-electrode nozzle.

elucidation of the effect of the electrode metal and thus the presence of the faradaic reactions do not require spray formation. It was found that after a considerable time (about several hours) or after a cleanup of the nozzle, the spray and leakage currents

obtained in the initial trial were considerably different from those measured in the trials after them. Therefore, the results for these initial trials are omitted here.

The results from the first set of experiments, the I-V characteristics, for three EA configurations (the stainless steel pin electrode with three different nozzle-electrode metals) are presented in Figure 7, where the measured spray current, I_S, the leakage current, I_L, and the total current, $I_T=I_S+I_L$, are presented. The corresponding results for the three configurations with the brass pin electrode are shown in Figure 8. The data presented in Figure 7 and 8 are the time averaged results with the standard deviation according to the multimeter recordings. Each result was taken for a span of 3 min in a steady state. Note, that the oil jet charge in all the experiments was negative, and thus, all the electric currents, while Figures 6 and 7 show their magnitudes. Also, the cathode voltage magnitude is used.
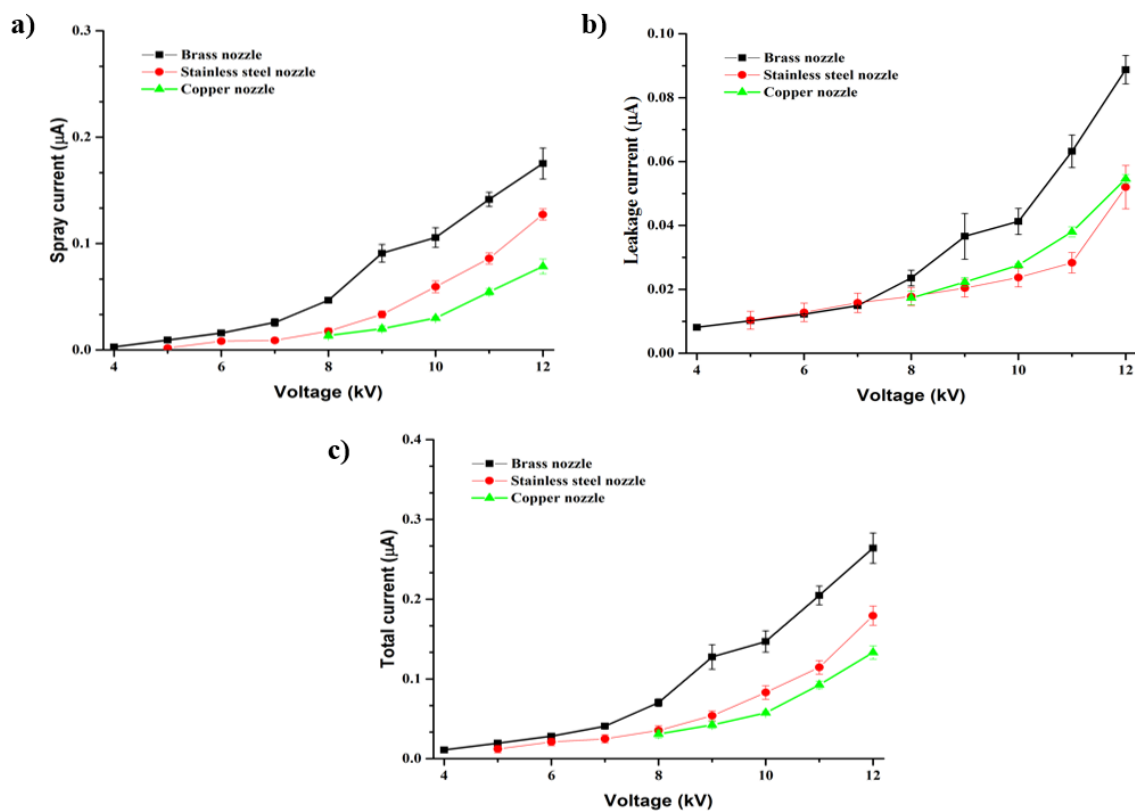
Figure 7. The electric current magnitudes (the time averaged values with the standard deviations) measured with the stainless steel pin electrode and three different counter-electrode metals using canola oil batch 1. Panels (a), (b) and (c) correspond to the spray current, I_S, the leakage current, I_L, and (c) the total current, I_T, in the cathode voltage magnitude up to 12 kV, respectively. The legends in the panels correspond to the counter-electrode nozzle metals. The flow rates in all the cases were kept at 0.9 mL/s. Measurements for copper counter-electrode nozzle at the voltage magnitudes below (in magnitude) - 8 kV were not conducted due to the sensitivity limits of the setup.

Figure 8. The electric current magnitudes (the time averaged values with the standard deviations) measured with the brass pin electrode and three different counter-electrode metals using canola oil batch 1. Panels (a), (b) and (c) correspond to the spray current, I_S, the leakage current, I_L, and (c) the total current, I_T, in the cathode voltage magnitude up to 12 kV, respectively. The legends in the panels correspond to the counter-electrode nozzle metals. The flow rates in all the cases were kept at 0.9 mL/s. Measurements for copper counter-electrode nozzle at the voltage magnitudes below (in magnitude) - 7 kV were not conducted due to the sensitivity limits of the setup.
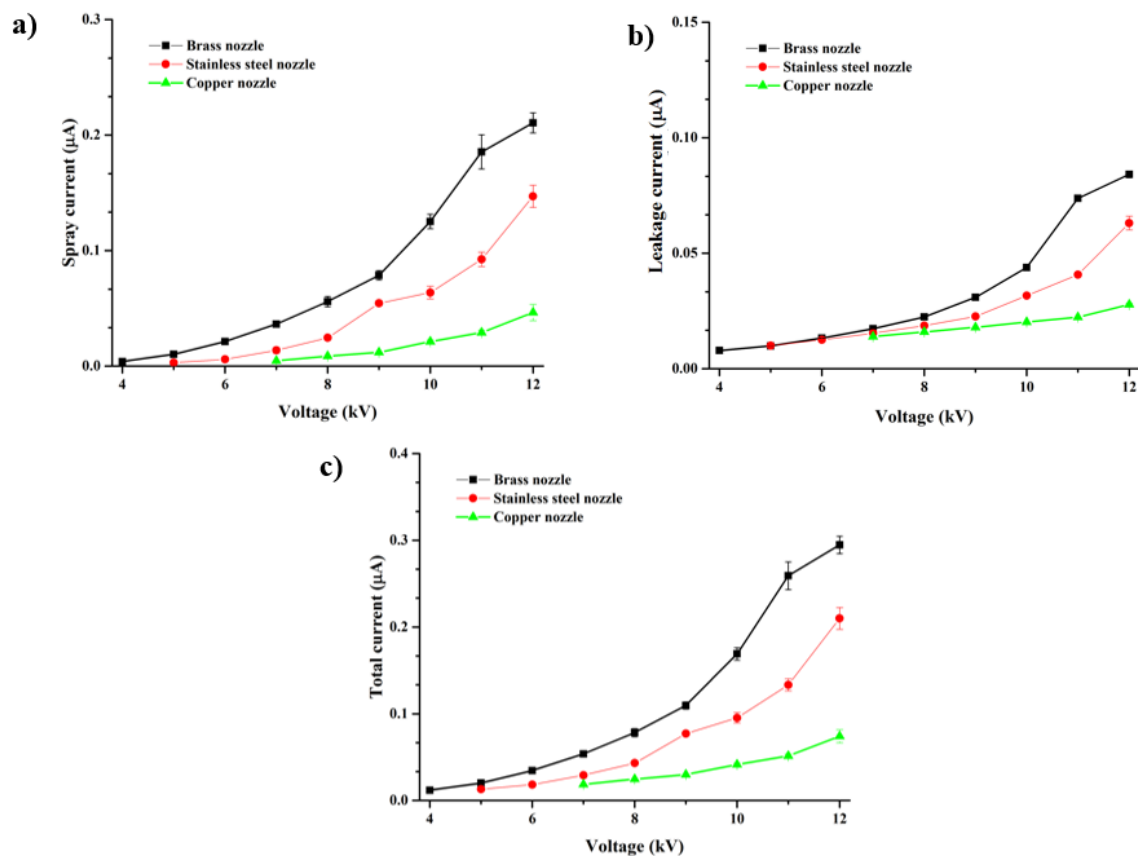
The results shown in Figures 7 and 8 reveal the effect of the electrode material on the electric current and thus, on the charge transfer. The differences between the results corresponding to different counter-electrode metals can hardly be attributed to any of the secondary factors introduced by the electrode manufacturing discussed in relation to the electrode characterization (the slightly different orifice radii and roughnesses), albeit this was not explored in detail. Note also, the material-related change in the charge transfer at the electrode surface is in full agreement with the presence of faradaic reactions. Faradaic reactions are treated in the framework of the general Volmer-Butler equation[29]

$$i = i_o \left\{ \exp\left[-\alpha\left(\frac{F}{RT}\right)V \right] - \exp\left[(1-\alpha)\left(\frac{F}{RT}\right)V \right] \right\} \tag{1}$$

where i is the electric current, R is the universal gas constant, T is the absolute temperature, V is the over-potential, α is the transfer coefficient, the pre-exponential $i_0 =$ nFk, with n being the number of electrons transferred, F being Faraday's constant, and k being the rate of faradaic reaction at the electrode.

Several in-depth superb overviews of the application and validity of the Volmer-Butler equation for different systems is available in literature[26, 29, 33], and as is shown below, the faradaic reactions in oil can also be described by this equation. Notably, the Volmer-Butler model predicts an increase in the magnitude of the total electric current with an increase in the magnitude of the applied voltages at the cathode, which is also observed in the present experimental data.

It should be emphasized that different tip radii and the shape imperfections prevent direct comparisons of the results corresponding to the two pin electrodes (made of stainless steel and brass).

The magnitudes of the charge per unit volume delivered by the electrified jet issued from the EA, the spray specific charge, $q_s=I_S/Q_v$, at -12.0 kV for the six different EA configurations are listed in Table 2.

Table 2. The magnitude of the spray specific charge for all six different EA configurations at the cathode voltage of -12.0 kV.

	Spray specific charge (C/m³)	
Counter-Electrode	Stainless Steel electrode	Brass electrode
Brass	0.19 ± 0.02	0.23 ± 0.01
Stainless Steel	0.14 ± 0.01	0.16 ± 0.01
Copper	0.09 ± 0.01	0.05 ± 0.01

The table shows that jet/spray electrification is significantly affected by the electrode material, and thus by faradaic reactions at the electrode surfaces. Accordingly, an EA can be optimized by the electrode material choice to achieve the highest specific charge, and thus to facilitate the dispersion and secondary atomization of the evaporating droplets in the spray, which would be formed at higher values of the charge per unit volume.

The Fixed Voltage Experiments. The second set of experiments was conducted to further verify the trends observed in the experiments of the first type described above. It should be emphasized that the experiments of the second type were not limited to single trials for each atomizer configuration. The voltage at the pin electrode (cathode) was fixed at -12 kV and all six atomizer configurations mentioned earlier were studied. Two additional canisters of food-grade canola oil were used in these experiments. The first of these canisters, denoted as batch 2, was used in combination with the stainless steel pin electrode along with all the three different metals of the counter-electrode nozzles. The second of these canisters of oil, batch 3, was used in combination with the brass pin electrode with all the three different metals of the counter-electrode nozzles. The benefit of conducting the experiments of this type at only one fixed voltage stemmed from the ability to measure multiple time series for the electric currents for each of the six atomizer configurations. In all the configurations the atomizer was operated for a total of 5 min, and the resultant spray, leakage and total currents were averaged with respect to time. Seven 5 min trials were conducted and the ensemble averages of all these trials for all atomizer configurations were obtained. The experiments of this type generate reliable statistics that allows one to further elucidate the effect of the nozzle material on the electric current value.

The flow rate remained nearly constant using the upgraded flow control, varying at times by no more than 3%. The resultant time averaged spray current, I_S, the leakage current, I_L, and the total current were ensemble averaged and are depicted in Figure 9.
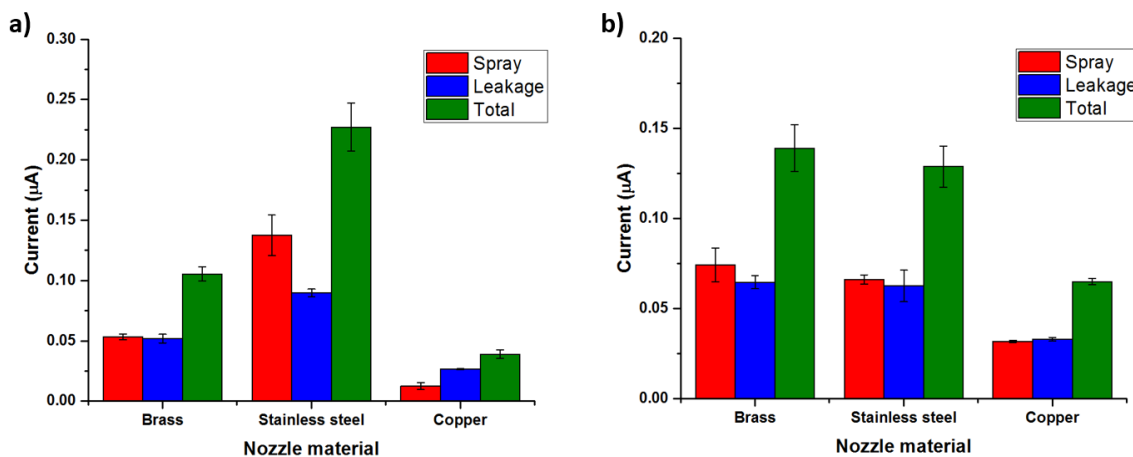
Figure 9. Magnitudes of the ensemble averaged spray, leakage and total currents measured for different counter-electrode nozzle materials with (a) stainless steel pin electrode and canola oil batch 2, (b) brass pin electrode and canola oil batch 3. The cathode voltage was -12 kV and the volumetric flow rate was 0.89 ± 0.02 mL/s.

Here also the effect of the counter-electrode material is clearly observed, which elucidates the role of the faradaic reactions at the electrode surfaces. This is in concert with the results of the experiments of the first type, the I-V characteristics experiments. Here again the copper counter-electrode nozzle results in significantly lower spray, leakage, and total currents regardless of the pin electrode material. Note however, that a different trend was observed in the experiments of the second type. Namely, when the stainless steel pin electrode was used, cf. Figure 9a, the highest total current observed was when a stainless steel counter-electrode nozzle was used. On the contrary, with the brass pin electrode, the highest total current was observed with the brass counter-electrode nozzle, cf. Figure 9b. In distinction, in the experiments of the first type, the

highest current was always achieved with the brass counter-electrode nozzle irrespective of the pin electrode material.

The difference between the trends in the experiments of the first and second type can also be attributed to the difference between oils used in them, namely, batches 1, 2 and 3, since the effect of the oil batch was quite significant, as the preliminary results demonstrated. It can be speculated that different oil batches have different concentrations of ions due to the differences in their manufacturing processes, and the nature of these charge carriers will be investigated in the future work. The results indicate two possible contributing factors: the original nature and concentration of the charge carriers in oil, and the type of faradaic reactions at the electrode surfaces (the latter includes not only the counter-electrodes but also the pin electrode, which was stainless steel for Figure 9a and brass for Figure 9b).

Theoretical Framework: The Volmer-Butler Model. Different mechanisms by which leaky dielectric liquids might be electrified in an EA have been reviewed in the monograph[16]. It is inferred from the discussion there that the electric field requirement for the Fowler-Nordheim tunneling or field emission in such liquids are higher than that for gases which is in the range of 10^9-10^{10} V/m. Streamer and vapor bubble formation in liquids like cyclohexane, isooctane, etc. have been discussed[16] and reviewed in detail along similar lines[34]. The studies involving formation of streamers[34] and bubbles[35] clearly involved the regime of corona discharge. Even the changes in the electrode tip after the experiments were reported[35]. Hence, it is desirable to avoid this regime. Therefore, such phenomena pertaining to the pre-breakdown phenomena, are not considered in the

present case. Even though the electro-chemical processes have been mentioned in relation to the EA operation[16, 27], no further details or confirmation have been provided. However, different regimes of the I-V characteristics in the study of dielectric breakdown in water have been discussed[36]. It was reported that there exist an exponential increase in the electric current with voltage due to electrolysis, a plateau region due to the formation of vapor and ultimately a drastic increase in the current due to the electron injection from metal. The I-V characteristics observed in the present work can be compared to the exponential regime similar to that of the prior work[33]. Hence, one can conclude that the normal operation of an EA is determined by the faradaic reactions at the electrodes.

The I-V characteristics discussed above can be described by the Volmer-Butler equation in its high over-potential (voltages) limit, namely the Tafel equation[26, 29, 33]. These I-V characteristics are similar to those measured in stagnant liquids[16]. Furthermore, recent studies on the EA performance involving vegetable oil and diesel oil also reveal similar trends[37, 38]. Accordingly, equation (1) in its high over-potential (voltages) limit reads[26, 29, 33]

$$i = i_o \exp\left[-\alpha\left(\frac{F}{RT}\right)V \right] \qquad (2)$$

The Tafel equation is found as the logarithm of Eq. (2) as

$$V = a + b \times \log i \qquad (3)$$

where,

$$a = \frac{2.3RT}{\alpha F}\log i_o \ , \quad b = -\frac{2.3RT}{\alpha F} \qquad (4)$$

Our experimental I-V characteristics for the brass pin electrode and brass counter-electrode plotted in the Tafel form is shown in Figure 10, where $i = I_T$, the total electric current.
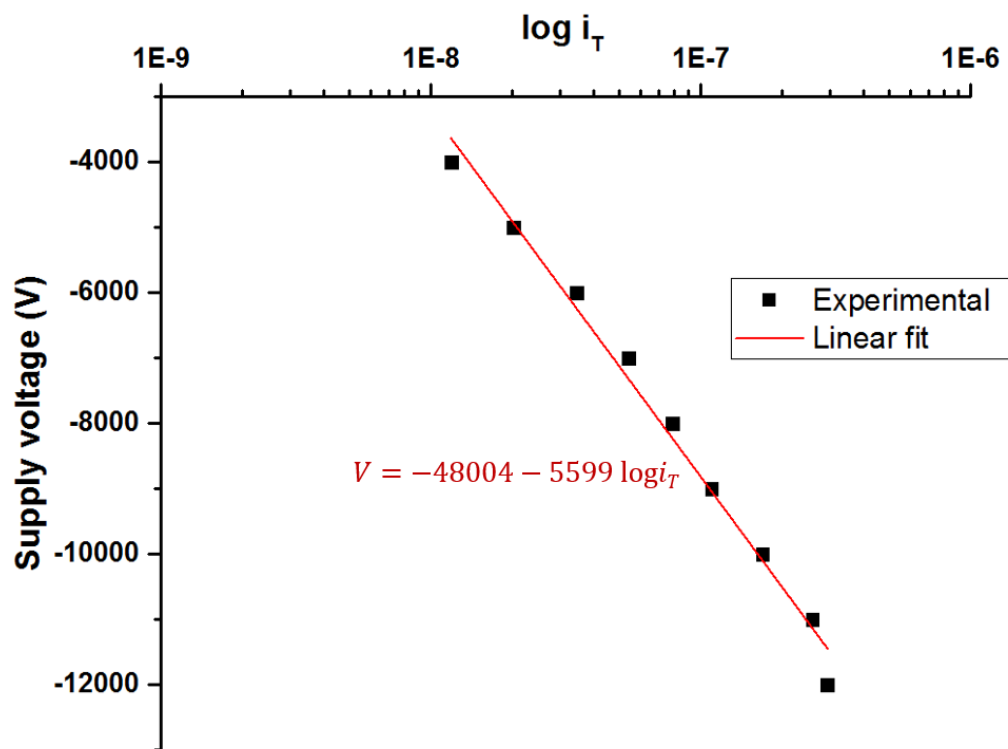

Figure 10. The I-V characteristics for the brass pin electrode and the brass counter-electrode approximated by the Tafel equation (cf. Figure 8).

The plot in Figure 10 yields the constant values as $i_0 = 2.7$ nA and $\alpha = 10^{-5}$. The value of i_0 represents the current order in both forward and reverse direction at electrodes when there is no applied voltage (i.e. without the net current) and is within the range of other electrochemical studies[29]. The transfer coefficient α is related to the energy barrier asymmetry between the reactants and the products of reaction. Theoretically, α ranges

from 0 to 1, however, for the liquids generally studied in electrochemistry[29] the value of α

lies between 0.3 and 0.7. The extremely low value of α found here may be attributed to

the nature of the faradaic reactions in oil, which is uncharted and deserves a further study.

Conclusion

The optimization of the electrostatic atomizers would require understanding and

control of both leakage and spray currents. This underlines the importance of

distinguishing the charge transfer mechanisms and their nature. Here we revealed the

evidence of the presence of faradaic reactions at the electrodes as the factor which

determine the total, spray and leakage electric currents. The effect of the electrode

material on the spray, leakage and total currents revealed by the experimental results in

this work elucidate the importance of the faradaic reactions at the electrode surfaces. The

regimes observed here were all kinetics-controlled and thus belong to the framework of

the slow discharge Volmer-Butler model in the Tafel limit (the high over-potential limit).

The rates of these reactions are also known to be voltage-controlled, and the results also

reveal this in the form of the electric currents significantly increasing with the magnitude

of the applied cathode voltage. It was also shown that the effect of the oil batch could be

quite significant for the results corresponding to any metal pairs chosen as the electrodes.

The investigation of the nature and the initial concentration of the charge carriers in oils,

and of the effect on them of the oil manufacturing process, is currently underway.

Namely, the detailed kinetics of faradaic reactions responsible for electrostatic charging

of oil is studied, the kinetic constants of the faradaic reactions are determined, as well as

the effect of pre-heating of oil on the concentration of charge carriers and its electric conductivity is measured.

Acknowledgement

References

[1] Inculet, I. I.; Tanasescu, F. T.; Cramariuc, R. (Eds.). The Modern Problems of Electrostatics with Applications in Environment Protection, Springer Science & Business Media, Heidelberg. 2012, 63, 363-377.

[2] Chang, J. S.; Crowley, J. M.; Kelly, A. J. (Eds.). Handbook of Electrostatic Processes, Dekkar, New York 1995.

[3] Crowley, J. M. Fundamentals in Applied Electrostatics, John Wiley & Sons, New York 1986.

[4] Melcher, J. R. Continum Electromechanics, MIT Press, Boston 1981.

[5] Shrimpton, J. S.; Yule, A. J. Electrohydrodynamics of charge injection atomization: regimes and fundamental limits, Atomiz. Sprays, 2003, 13, 173-190.

[6] Vesely, P. W.; Shrimpton, J. S.; Mashayek, F.; Schick, R. J.; Thenin, M. Spray analysis of a multi-orifice electrostatic atomization nozzle with high viscosity vegetable

oils, 13th International Conference on Liquid Atomization and Spray Systems, Tainan, Taiwan, Aug. (2015).

[7] Yule, A. J.; Shrimpton, J. S.; Watkins, A. P.; Balachandran, W.; Hu, D. Electrostatically atomized hydrocarbon sprays, Fuel, 1995, 74, 1094-1103.

[8] Kim, K.; Turnbull, R. J.; Generation of charged drops of insulating liquids by electrostatic spraying. J. Appl. Phys. 1976, 47, 1964-1969.

[9] Lord Rayleigh. The equilibrium of liquid conducting masses charged with electricity, *Phil. Mag.* 1882, 14, 184-186.

 [10] Taflin, D. C.; Ward, T. L.; Davis, E. J. Electrified droplet fission and the Rayleigh limit. *Langmuir*, 1989, 5, 376-384.

[11] Duft, D.; Achtzehn, T.; Muller, R.; Huber, B.A.; Leisner, T. Coulomb fission: Rayleigh jets from levitated microdroplets. Nature 2003, 421, 128-128.

[12] Ferraro, P.; Coppola, S.; Grilli, S.; Paturzo, M.; Vespini, V. Dispensing nano-pico droplets and liquid patterning by pyroelectrodynamic shooting. Nature Nanotechnology, 2010, 5, 429-435.

[13] Grilli, S.; Miccio, L.; Gennari, O.; Coppola, S.; Vespini, V.; Battista, L.; Orlando, P.; Ferraro, P. Active accumulation of very diluted biomolecules by nano-dispensing for easy detection below the femtomolar range. Nature Communications, 2014, 5, 1-6.

[14] Robinson, K. S.; Turnbull, R. J.; Kim, K. Electrostatic spraying of liquid insulators. IEEE Trans. on Industry Applications, 1980, IA-16, 308-317.

[15] A. J. Kelly, The electrostatic atomization of hydrocarbons, J. of the Institute of Energy, 1984, 57, 312-320.

[16] Shrimpton, J. S. Charge Injection Systems: Physical Principles, Experimental and Theoretical Work. Springer Science & Business Media, Heidelberg, 2009.

[17] Shrimpton, J. S.; Yule, A. J. Characterization of charged hydrocarbon sprays for application in combustion systems. Exp. Fluids, 1999, 26, 460-469.

[18] Rigit, A. R. H.; Shrimpton, J. S.; Spray characteristics of charge injection electrostatic EAs with small-orifice diameters. Atomiz. Sprays 2006, 16, 421-442.

[19] Malkawi, G.; Yarin, A. L.; Mashayek, F. Breakup mechanisms of electrostatic atomization of corn oil and diesel fuel. J. Appl. Phys. 2010, 108, 064910.

[20] Patel, V. K.; Seyed-Yagoobi, J.; Sinha-Ray, S.; Sinha-Ray, S.; Yarin, A. L. Electrohydrodynamic conduction pumping-driven liquid film flow boiling on bare and nanofiber-enhanced surfaces. J. Heat Transf. 2016, 138, 041501.

[21] Zussman, E.; Theron, S. A. Electric and magnetic parameters in liquids and gases. Section 3.7 in Springer Handbook of Experimental Fluid Mechanics (Editors C. Tropea, A. L. Yarin, J. F. Foss), 2007, 159-169.

[22] Castellanos, A.; Perez, A. T. Electrohydrodynamic systems. Chapter 21 in Springer Handbook of Experimental Fluid Mechanics (Editors C. Tropea, A. L. Yarin, J. F. Foss), 2007, 1317-1333.

[23] Melcher, J. R.; Taylor, G. I.; Electrohydrodynamics: a review of the role of interfacial shear stresses. Annu. Rev. Fluid Mech. 1969, 1, 111–146.

[24] Saville, D. A. Electrohydrodynamics: The Taylor-Melcher leaky dielectric model. Annu. Rev. Fluid Mech. 1997, 29, 27-64.

[25] Kourmatzis, A.; Ergene, E. L.; Shrimpton, J. S.; Kyritsis, D. C., Mashayek, F.; Huo, M. Combined aerodynamic and electrostatic atomization of dielectric liquid jets, Exp. Fluids, 2012, 53, 221-235.

[26] Levich, V. G. Physicochemical Hydrodynamics. Prentice Hall, Englewood Cliffs, 1962.

[27] Alj, A.; Denat, A.; Gosse, J. P.; Gosse, B.; Nakamura, I. Creation of charge carriers in nonpolar liquids. Electrical Insulation, IEEE Transactions on Electrical Insulation 2 1985: 221-231.

[28] Zhang, Y.; Yarin, A. L. Electric current and irreversible faradaic reaction on electrode in contact with electrolyte, J. Electrochem. Soc., 2012, 159, H787–H791.

[29] Bard, A. J.; Faulkner, L. R. Electrochemical Methods: Fundamentals and Applications, John Wiley & Sons, New York, 2001.

[30] Cardarelli, F. Materials Handbook: A Concise Desktop Reference. Springer Science & Business Media, 2008

[31] Trasatti, S. Work function, electronegativity, and electrochemical behaviour of metals: II. Potentials of zero charge and "electrochemical" work functions. Journal of Electroanalytical Chemistry and Interfacial Electrochemistry, 1971, 33, 351-378.

[32] Haynes, W. M. The CRC Handbook of Chemistry and Physics 93RD Edition, 2012. Chemical Rubber Company.

[33] Antropov, L.I. Theoretical Electrochemistry. Honolulu University Press of the Pacific, Honolulu, 2001.

[34] Kolb, J. F.; Joshi, R. P.; Xiao, S.; Schoenbach, K. H. Streamers in water and other dielectric liquids. Journal of Physics D: Applied Physics, 2008, 41, 234007.

[35] Kattan, R.; Denat, A.; Bonifaci, N. Formation of vapor bubbles in nonpolar liquids initiated by current pulses. IEEE transactions on electrical insulation, 1991, 26, 656-662.

[36] Szklarczyk, M.; Kainthla, R. C.; Bockris, J. O. M. On the dielectric breakdown of water: an electrochemical approach. J. Electrochem. Soc., 1989, 136, 2512-2521.

[37] Malkawi, G. Point-to-plane and Plane-to-plane Electrostatic Charge Injection Atomization for Insulating Liquids. (Doctoral dissertation, University of Illinois at Chicago) 2010.

[38] Ergene, E. L. Investigation of the Electrostatic Atomization Method for Remote Injection and High Pressure (Doctoral dissertation, University of Illinois at Chicago), 2012.